Exp Fluids (2007) 42:955–970
DOI 10.1007/s00348-007-0318-y

RESEARCH ARTICLE

Time resolved analysis of steady and oscillating flow in the upper human airways

S. Große · W. Schröder · M. Klaas · A. Klöckner · J. Roggenkamp

Received: 5 December 2006 / Revised: 13 April 2007 / Accepted: 20 April 2007 / Published online: 27 May 2007
© Springer-Verlag 2007

Abstract In this experimental study a thorough analysis of the steady and unsteady flow field in a realistic transparent silicone lung model of the first bifurcation of the upper human airways will be presented. To determine the temporal evolution of the flow time-resolved particle-image velocimetry recordings were performed for a Womersley number range $3.3 \leq \alpha \leq 5.8$ and Reynolds numbers of Re_D = 1,050, 1,400, and 2,100. The results evidence a highly three-dimensional and asymmetric character of the velocity field in the upper human airways, in which the influence of the asymmetric geometry of the realistic lung model plays a significant role for the development of the flow field in the respiratory system. At steady inspiration, the flow shows independent of the Reynolds number a large zone with embedded counter-rotating vortices in the left bronchia ensuring a continuous streamwise transport into the lung. At unsteady flow the critical Reynolds number, which describes the onset of vortices in the first bifurcation, is increased at higher Womersley number and decreased at higher Reynolds number. At expiration the unsteady and steady flows are almost alike.

1 Introduction

The lung as the human respiratory organ consists of a repeatedly bifurcating network of tubes with progressively decreasing diameters. The understanding of the highly unsteady and non-linear flow field within these tubes is of great importance to interpret particle deposition patterns and thus to develop aerosol drug delivery systems (Comer et al. 2000, 2001a, b; Martonen 2001; Mochzuki 2003). Furthermore, utilizability and efficiency of artificial lung ventilation highly depends on the velocity and pressure distribution, both of which are associated with a specific ventilation strategy. Despite numerous experimental and numerical investigations having been conducted so far it has to be stated that there still exists a considerable amount of uncertainty concerning the very complex flow field in the human lung. This is mainly due to the high intricacy of the human lung geometry. In other words, results for realistic models of the lung are still rare. The majority of experimental and numerical investigations has been performed using models with a simplified geometry which might lead to flow fields that deviate considerably from realistic lung flows. For this reason, results could often not explain the fluid-mechanical causes for certain particle deposition patterns or non-linear lung flow phenomena.

One of the earliest publications by Schroter and Sudlow (1969) focused on velocity profiles and flow patterns in symmetric bifurcating geometries. The authors used hot-wire probes and smoke visualizations techniques assuming a steady air flow in rigid tubes with smooth surfaces. These assumptions are commonly made with reference to the existing local Reynolds number based on the mean geometry diameters in the range of Re_D = 500–2,000 and Womersley numbers of about 5–25, which are typical values for normal breathing conditions. As far as the influence of the Reynolds number on the characteristics of the flow structures during inspiration is concerned, Martonen et al.(2001) as well as Grotberg (2001) report a strong dependence of the flow field on the

S. Große (✉) · W. Schröder · M. Klaas · A. Klöckner · J. Roggenkamp
Institute of Aerodynamics, RWTH Aachen University, 52062 Aachen, Germany
e-mail: s.grosse@aia.rwth-aachen.de

Reynolds number in the Reynolds number range of Re = 200–2,000 and Re = 200–1,200, respectively. On the other hand, Liu et al. (2003) found comparable flow patterns by numerically investigating an asymmetric human lung airway system for Reynolds numbers between 400 and 1,600. Furthermore, there is no common consensus on the impact of the entry flow profiles on the flow structures evolving in the upper lung. While some investigators report the bifurcation flow phenomena to be independent of the inflow conditions, Yang et al. (2006) report a strong impact of different inflow conditions on the flow in the subsequent bifurcation zones. The rather complicated flow field downstream of the laryngeal region has recently been investigated in Ball et al. (2006) by a Lattice–Boltzmann method showing strong vortex shedding with an impact 7–8 trachea diameters downstream of the laryngeal region and as such in the bifurcation region.

Since the flow between consecutive bifurcation regions cannot fully develop in a natural lung geometry, the upstream condition within the network of bifurcations influences the flow structures further downstream. Nevertheless, a great number of investigations have been performed for artificial geometries with rather long branches between subsequent bifurcations.

Experimental investigations of Ramuzat and Riethmuller (2002) concentrated on a plane symmetric model of subsequent pipe bifurcations, hence introducing a major simplification of the model geometry. In their experiments, oscillating flow phenomena have been investigated for different Womersley numbers emphasizing the temporal development of the velocity through successive bifurcations and the quasi-steadiness of the flow for low oscillation frequencies.

Recent numerical calculations focused on the analysis of aerosol transport and particle disposition patterns and have been carried out by numerous groups, e.g., Leong et al. (2005), and Robinson et al. (2006). Comer et al. (2000, 2001a, b) investigated the flow structure in symmetric double-bifurcations under steady conditions in a system consisting of three subsequent bifurcations. The Reynolds number based on the pipe-diameter varied from Re_D = 500–2,000. The authors detected strong vortical flow fields especially in the region of the second bifurcation leading to complex particle distributions and deposition patterns. The flow in a plane and non-symmetric bifurcation has been calculated by Liu et al. (2003). Their simulations comprised the flow field from the fifth to the 11th branch of the model of Weibel (1963) resulting in Reynolds numbers in the range of Re_D = 200–1,600. All the aforementioned models were based on the planar character of the pipe network. Furthermore, most of the studies were performed for highly symmetric models with bifurcations that divide the lower generations' pipe into two subsequent tubular pipes with nearly or exactly likewise diameter.

Recently, experimental and numerical studies have been carried out for non-planar lung geometries. Caro et al. (2002) investigated steady inspiratory flow in a symmetric model of the lung with two generations. For planar and non-planar configurations the results emphasized the different development of the flow fields and volumetric distributions between varying types of geometry. The distribution of the wall-shear stress in the different generations of the bronchia was measured by optically visualizing the reaction between acid vapor and blue litmus coatings in the bronchial system. It was concluded that inspiratory flow in larger human bronchial airways is asymmetric and swirling with implications for all transport processes including those of particles. A similar model has been used in a numerical simulation by Comer et al. (2000). The findings show that for the out-of-plane configuration of the different generations of the bronchia the particle deposition patterns differed from the planar case and possessed higher particle efficiencies for diluted suspensions of inhaled particles where the efficiency is defined as the number of particles deposited in a certain section divided through the total number of particles entering the region.

Numerical results for the most complicated and realistic model of the lung geometry have been presented by van Ertbruggen et al. (2005). The results evidenced the highly three-dimensional character of the flow field emphasizing the importance of non-fully developed flows in the branches due to the relatively short lengths.

The findings in the literature show that physically relevant studies of the bronchial airway anatomy and the corresponding flow field require realistic and thus complex models of the lung geometry. On the one hand, this challenge can be pursued by defining an artificial lung model with high complexity, taking into account the three-dimensional characteristics of the branches, e.g., asymmetry of the bifurcation zones, the 'natural' ratio between the cross sections of subsequent generations of branches, the non-circular shape of real bronchia, and the impact of the upstream flow conditions on the mass flow distributions in sub-branches. On the other hand, a realistic lung model can be derived from original, hence exact, lung geometry data. Modern clinical image-recording techniques allow the exact determination of the lung geometry at least for the first six to ten bronchial branches. This offers the possibility to manufacture a 'negative' kernel of the human airways made from solvable materials, which can be used to generate transparent silicone models ('positive'). This approach finally leads to a realistic model of the human lung providing optical access to the airways. The difficulty in such 'natural' models is the lack of symmetry and

orientation such that a fully three-dimensional investigation of the flow field is a must to adequately describe the flow structures.

It has to be mentioned, however, that some compromises concerning the so-called realistic model were accepted in this experimental study. The inflow condition was a fully developed laminar profile. The experimental setup does not completely mimic the laryngeal and tracheal region. Furthermore, it will be necessary to simulate a more realistic outflow condition with individual pressure distributions at the end of the 6th generation branches.

The objective of this study is to perform detailed velocity measurements in the first bifurcation of the above-described realistic lung model using standard and time-resolved particle-image velocimetry (PIV). The first experiments allow to analyze the flow patterns in the first bifurcation of the human lung consisting of the trachea and the first bronchia generation.

The results of the present study mainly serve to fundamentally understand the time-dependent development of the flow field within the upper bifurcations of the human lung under normal breathing conditions. However, unlike the investigation of Große et al. (2007) not only steady but also unsteady flow fields will be measured. Future studies will especially focus on the influence of different ventilation strategies on the flow field within the lung bifurcations and particularly on the pressure distribution in the lower respiratory system.

High-frequency oscillatory ventilation (HFV) using ventilation frequencies between 5 and 15 Hz has reached increasing clinical application, since it showed to have a benign effect on the gas-exchange efficiency and a less detrimental physiological impact. Nonetheless, the reason for this is hardly understood and hence, measurements under high-frequency oscillatory ventilation conditions, which will be performed in the context of the ongoing research project, will help to identify the differences in the flow structure and pressure distribution during HFV in comparison with the flow field developing under natural respiration conditions, the determination of which is the focus of the present study.

Therefore, steady inspiration and expiration flows have been studied for a variety of Reynolds numbers based on the trachea diameter D ranging from Re_D = 1,250 to 1,700. Since the model extends to the 6th generation the effect of upstream bifurcations on the expiration flow can be investigated. Additionally, oscillating flow with Reynolds numbers ranging from Re_D = 1,050 to 2,100 and Womersley numbers α ranging from 3.3 to 5.8, where the Womersley number is defined as $\alpha = 0.5D\sqrt{2\pi f/\nu}$, was investigated. Herein, the quantity D denotes the diameter of the trachea, f is the frequency of the ventilation cycles, and ν represents the kinematic viscosity of the fluid. The time-resolved measurements have been performed in a center plane in the first bifurcation region of the lung geometry, such that the temporal evolution of the flow field in the first lung bifurcation during a complete breathing cycle could be investigated.

In the following sections, first the experimental setup is described in great detail. Then, the results for steady and time-dependent flows are discussed. Finally, some conclusions wrap up this paper.

2 Experimental setup

2.1 Lung model

The PIV experiments were conducted in a realistic, three-dimensional lung model that extends to the 6th generation of the bronchial system. It is fabricated from transparent silicone (RTV815) to allow perfect optical access. Figure 1a depicts a picture of the hollow lung model in the silicone block. The complete lung geometry is indicated in Fig. 2 by showing several cross sections. At inspiration the fluid enters the lung model through an anatomically shaped trachea as illustrated in Fig. 1b. The flow exits the model through channels that have been drilled from the 6th

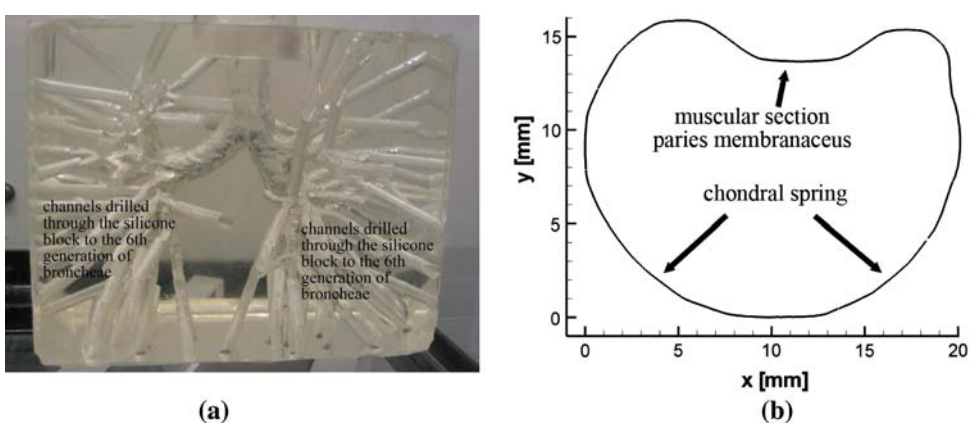

Fig. 1 **a** Picture of the hollow lung model in silicone. **b** Sketch of the cross section of the trachea (plane normal to the average direction of the trachea, oriented 25.0° to the z-direction from Fig. 2)

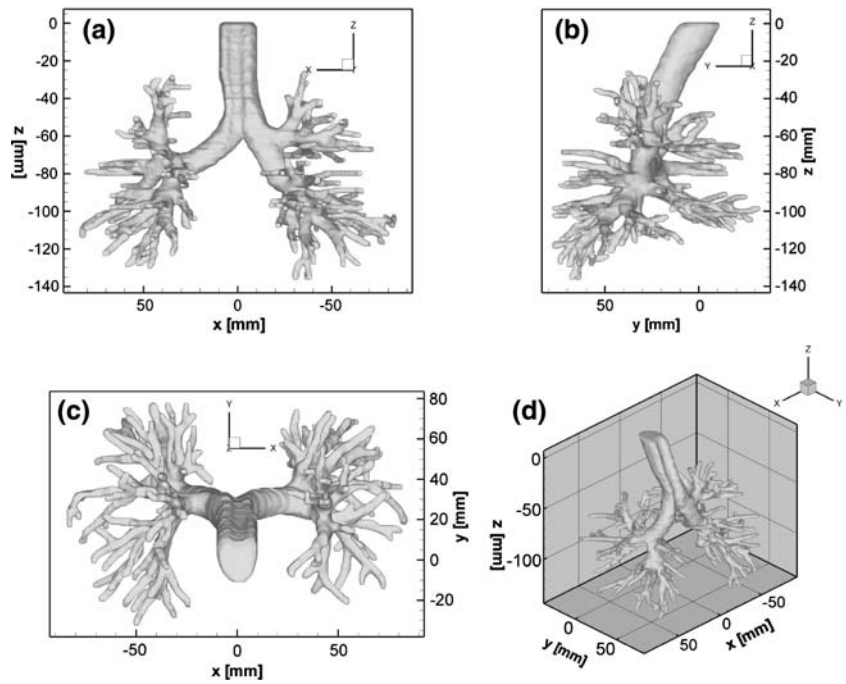

Fig. 2 Illustrations of the realistic lung model. **a** Dorsal or back view, **b** lateral view, and **c** caudal or top view; **d** isometric view

generation's endings through the block sides. The trachea of the model possesses the typical shape of a natural trachea with a dorsal indentation. The real human trachea is stiffened by chondral springs in the ventral part of the cross section. The dorsal, i.e., the back part of the trachea consists of a muscular structure (paries membranaceus) and allows a widening of the trachea.

2.2 In- and outflow conditions

The choice of an appropriate inflow condition is crucial for the investigation of the lung flow since the velocity profile in the trachea has a strong impact on the flow field in the first lung bifurcation (Yang et al. 2006). To enable a comparison with numerical results and with future computations a defined inflow condition in the trachea was chosen. Most numerical calculations use a classical and fully developed laminar profile as inflow condition. Also, parallel flow profiles have been investigated. To uniquely define the inflow characteristics and to ensure a fully developed velocity profile, an L = 500 mm long pipe section with a constant cross-section matching that in the upper part of the trachea was modeled. The hydraulic diameter in the model D is approximately 18.3 mm leading to a ratio of L/D = 27. The Reynolds number based on the hydraulic diameter of the trachea ranges from Re_D = 1,250 to 1,700 for the steady flow experiments. This results in a fully developed laminar profile at the inlet. Choosing an anatomically shaped trachea instead of a plain pipe flow helps to prevent flow separation in the lung inflow region by avoiding the discontinuous change of the cross section at the junction between the inflow pipe section and the trachea. At any rate such a geometry would generate unphysical disturbances of the flow field further downstream of the bifurcations.

Note, that the human trachea possesses a total length of 10–12 cm, measured from the laryngeal region (cartilage cricoidea) to the first bifurcation (bifurcation tracheae). Hence, the flow entering the bifurcation will be strongly influenced by the geometry of the upper airways and the perturbations caused by the larynx region. Thus, the real flow in the human body cannot be considered fully developed.

The flow exits into a net of pipes, which have the same diameter as the branches of the 6th generation of the lung model. They were drilled into the silicone block such that they can be considered straight extensions of these branches. Due to the fact that the vertical pressure in the tank complies with the hydrostatic pressure distribution it can be assumed that the outlet pressure in the experiment is nearly constant for all branches of the 6th generation exiting into the tank.

Measurements at steady inspiration and expiration have been performed using a closed-circuit flow facility. Note that the experimental setup is identical for both cases except for the flow direction. For either setup the fluid supply for the tank has to be carefully positioned since a homogeneous flow circulation has to be guaranteed for an idealized flow distribution in the lung model. Measurements at oscillating flow, which were designed to simulate a breathing cycle, have been conducted with an open-circuit flow facility. In this case, a sinusoidal fluid movement was realized using a piston driven by an eccentrically supported

rod. Figure 3a, b show schematics of the experimental setup for steady and oscillatory flow.

2.3 Flow parameters

A water/glycerine mixture with a refractive index of $n = 1.44$ being identical to that of the silicone block was used as flow medium. The dynamic viscosity of the mixture with 60.7 mass percent glycerine is $\eta = 10.3 \times 10^{-3}$ Pa s and the density $\rho = 1.153 \times 10^3$ kg/m^3 for the temperature during the experiments.

The Reynolds number Re_D for the steady flow measurements varied between 1,250 and 1,700. The Reynolds number Re_D for oscillatory flow based on the maximum flow velocity during inspiration varied between 1,050 and 2,100. The Womersley number range was 3.3–5.8. Hence, typical human breathing cycles under normal conditions can be simulated with this setup. A list of characteristic flow parameters of the different measurements is given in Table 1.

2.4 Tracer particles

Hydrogen bubbles generated in an electrolytic unit upstream of the trachea were used as tracer particles. Since the amount of bubbles in plain water/glycerine is rather low due to missing electrolytes in the fluid a very small amount of saline additive is mixed into the fluid. The electrolytic unit was especially designed to avoid flow disturbances upstream of the trachea.

The size of the tracer particles depends on the electrolytic voltage, the distance between the metal cathode and anode of the electrolytic unit, and the mean flow velocity through the unit. The distance and voltage were adjusted to achieve an optimized size of the bubbles of 1–5 μm. Due to the laminar flow in the trachea it was necessary to start the electrolytic unit at least 5 min prior to the measurement series to generate a homogeneous distribution of particles. At very low Reynolds numbers it was necessary to switch off the unit during the measurements since bubbles were not torn off the metal surfaces by the low flow velocities but accumulated at the edges of the unit yielding too large tracer particles.

The use of hydrogen bubbles was necessary since standard flow particles (PA, etc.) led to heavy particle deposition on the walls of the lung model resulting in strong reflections at the boundaries of the bronchial system and as such in a significantly reduced quality of the images. However, first experiments done with solid particles showed flow structures comparable to those measured with hydrogen bubbles. Nevertheless, the use of solid tracer particles and hence the contamination of the model led to a considerably higher number of invalid vectors in the measured velocity fields. The lifespan of the bubbles is in the range of 5–10 min such that for expiration the electrolytic unit could be kept in the same position in the flow circuit still ensuring a sufficient number of bubbles for the PIV measurements under reversed flow conditions.

2.5 Measurement equipment and image evaluation

In all measurements a standard PIV system was used consisting of a double cavity Minilite Nd:YAG-Laser with a nominal power of 25 mJ, a PCO SensiCam QE double-shutter camera with a resolution of 1,376 × 1,040 px, and a lens with an aperture of 1.8 to reduce the depth of focus to a minimum and to maximize the available light. To gain some first knowledge of the spatial evolution of the flow field in the first bifurcation during steady inspiration, experiments

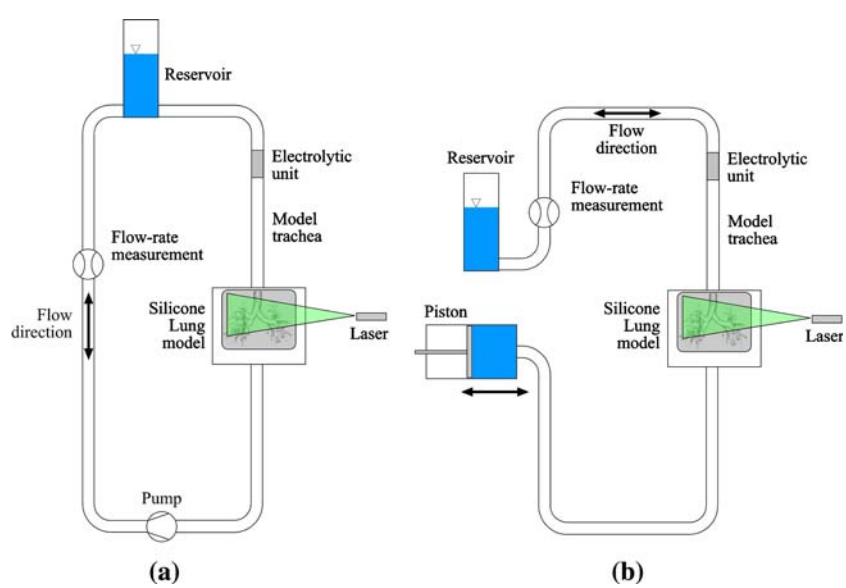

Fig. 3 **a** Schematic of the experimental setup for steady flow. **b** Schematic of the experimental setup for oscillating flow

Table 1 Flow parameters

Parameter	Multi-plane	Steady inspiration	Steady expiration	Oscillating flow
Reynolds number Re_D	1,700	1,250–1,700	1,250–1,700	1,050–2,100
Mean trachea bulk velocity U_{mean} (m/s)	0.83	0.60–0.83	0.60–0.83	–
Maximum trachea bulk velocity U_{max} (m/s)	–	–	–	0.50–1.10
Womersley number α	0	0	0	3.27–5.77
Volumetric flow per cycle V (cm^3)	–	–	–	90.6–570
Frequency (cycles/min)	–	–	–	10.85–34.5

were performed at a Reynolds number of $Re_D = 1{,}700$ using a set of parallel light sheets with a spacing of 1 mm and a field of view of 95.8 × 72.4 mm. Next, 500 images were taken at a frequency of 2 Hz for steady inspiratory and expiratory flow in a streamwise oriented central plane of the bifurcation. The field of view for these measurements was approximately 74.6 × 56.4 mm. Based upon these results the temporal development of the flow structures in the left bronchia was investigated in detail with time-resolved PIV at a frame rate of 8 Hz and a field of view of approximately 72.4 × 27.7 mm. In this case 200 images were taken for each set of Womersley and Reynolds number. Thus, depending on the specific parameter combination a minimum of 4–14 complete inspiration and expiration cycles per experiment were captured.

The data was post-processed using the commercial VidPIV 4.6 PIV software by ILA GmbH. A multi-pass correlation was applied starting with a 64 × 64 px interrogation size with 50% overlap followed by an adaptive cross correlation with a final 16 × 16 px interrogation window size leading to a vector spacing of 0.7 mm for the time-resolved measurements. Thus, approximately 25 vectors across the diameter of the first generation of bronchia could be achieved. Only weak local reflections from the walls allowed to exactly determine the bronchial structure.

The dynamic range in the PIV images was up to 4,096 gray scales and 4–6 particles per interrogation area led to a high accuracy of the adaptive correlation routines. Due to an achievable sub-pixel accuracy of less than 0.02 px of the routines under these conditions the accuracy in the velocity determination was better than 0.5%. To determine the pulse distance at oscillating flow was rather difficult since the setting must be adapted to maximum inspiration or expiration flow velocities as well as to the quasi-static conditions at flow reversal.

3 Results

To obtain some knowledge about the global structure of the flow field in the bifurcation of the trachea and bronchia, first experiments were performed in Sect. 3.1.1 for steady inspiration at a constant Reynolds number of $Re_D = 1{,}700$. Due to the complexity of the velocity field in the bifurcation region the flow was recorded in thirteen parallel, vertical lightsheets with a lateral displacement of 1 mm, hence covering the complete cross section of the bronchia. This allowed the reconstruction of three-dimensional flow phenomena from the two-dimensional velocity distributions. Based on the results of these measurements, experiments were conducted in Sect. 3.1.2 for steady inspiration and expiration at two different Reynolds numbers of $Re_D = 1{,}250$ and $Re_D = 1{,}700$ to determine the influence of the Reynolds number on the flow field.

To investigate the temporal and spatial evolution of the flow structures during a breathing cycle measurements were performed for a set of combinations of Reynolds number Re_D and Womersley number α in Sect. 3.2.1 and 3.2.2. The oscillating flow was generated by imposing a sinusoidal flow rate with zero mean velocity as described in Sect. 2.

The results from the three-dimensional reconstruction of the steady flow field evidence that global geometric characteristics of the flow field developing in the lung bifurcation can be derived from an investigation of one single plane in the center plane of the bifurcation. Especially the radial and streamwise dimension of the vortical regions developing at the inner curve of the bifurcation can be deduced from the single plane measurements. It goes without saying that time-resolved three-dimensional measurements are required to study the flow field in detail. This, however, is beyond the scope of the present investigation.

Figure 4 illustrates the positions and sizes of the measurement planes with respect to the lung geometry for all cases investigated. The notations 'left' and 'right' used in the following discussion of the findings are defined for dorsal view on the upper human airways complying with the usual notation in anatomy.

3.1 Steady flow analysis

3.1.1 Multi-plane measurements

Figure 5 illustrates the two-dimensional velocity distributions in the first bifurcation during steady inspiration at

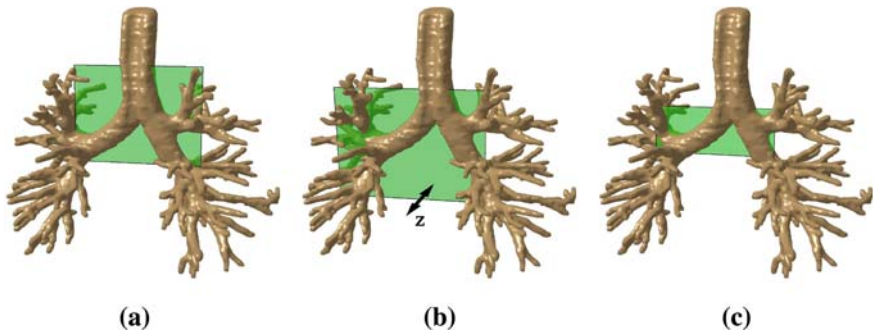

Fig. 4 Measurement planes in dorsal view for **a** multi-plane measurements (only one plane is illustrated), **b** steady, and **c** oscillating flows

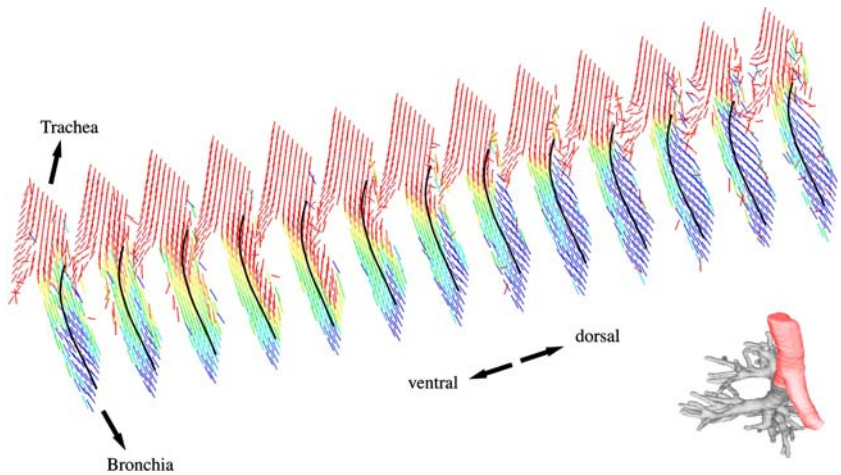

Fig. 5 Two-dimensional velocity distributions in the first bifurcation during steady inspiration at a Reynolds number of Re_D = 1,700 in parallel planes. Vector color qualitatively emphasizes *u*/*w*. The *black line* represents the extension of the region containing the counter-rotating vortices

a Reynolds number Re_D = 1,700 in parallel planes. The vector fields evidence a zone with a strongly reduced streamwise velocity component at the upper wall of the left bronchia, which is slightly skewed in the ventral direction. This asymmetry results most likely from the angle between the central planes of the trachea and bronchia and hence from the torsion of mother and daughter branches of the bifurcation. Since the terminus 'separation' usually denotes a region containing reversed flow, it can not be applied to describe the flow structure identified in the measurements. Although the mean streamwise velocity is strongly reduced within these regions and especially near the side walls, no flow recirculation could be evidenced. Since the measurement planes cover the whole cross section of the bronchia the three-dimensional shape of the region of secondary flow structures can be determined. The complete flow pattern is depicted in Figs. 6 and 7. The measurements indicate that two counter-rotating vortices form inside the region of reduced velocity. The fluid flows along the outer walls of the bronchia to the central plane and then to the centerline towards the high-speed region on the inner curve of the bifurcation. This fluid motion is superposed with fluid transport in the downstream direction generating a spiral-like shape of the vortices. The multi-plane measurements also reveal that the measurements only in the central plane allow the reconstruction of the spatial extent of the counter-rotating vortices with sufficient accuracy.

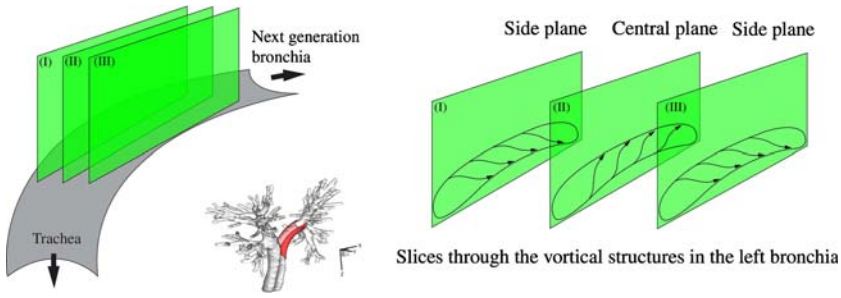

Fig. 6 Schematic of the two-dimensional measurement planes in the first bifurcation at three distinct positions

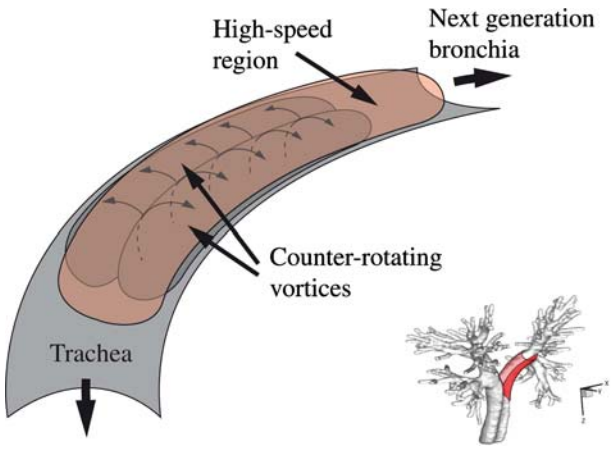

Fig. 7 Schematic of the two counter-rotating vortices evolving along the outer bifurcation. The high-speed region is illustrated in *red*

3.1.2 Steady inspiration and expiration

Figure 8a, b show a smooth laminar velocity profile from the trachea entering the bifurcation zone at inspiration. The figures illustrate the velocity magnitude and some velocity profiles for selected positions in the bifurcation, which evidence a large zone of strongly reduced velocity in the left bronchia and strongly skewed velocity distributions. This area is located at the inner curve of the bifurcation and extends to the bronchia centerline. As discussed above two counter-rotating vortices exist in this region. These secondary flow phenomena resemble spiral-like structures moving the fluid from the center of the bronchia sidewards to the upper wall of the bifurcation and back to the central region of the bronchia. The fluid captured in these vortical structures is still transported along the bronchia, but with a reduced mean volumetric flow rate. This causes the remaining flow to form a jet-like high speed region along the lower curve of the bifurcation.

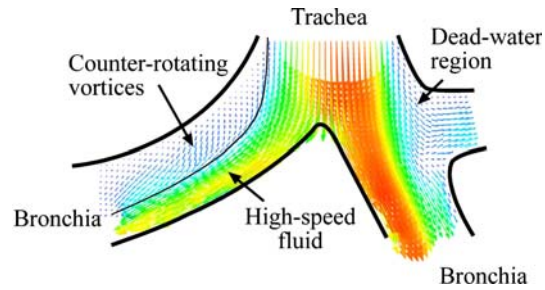

Fig. 9 Flow structure in the center plane of the first bifurcation at maximum inspiration. Vector length and color show the velocity magnitude

Figure 9 shows the instantaneous flow pattern evidencing the transport of the fluid in the center plane. A schematic of the overall flow structure in the left bronchia illustrating the counter-rotating vortices was already depicted in Fig. 7. As a consequence of the high velocities near the lower wall of the bifurcation a strong shear layer evolves. A similar behavior can be observed in the right bronchia, although the intensity and extension of the corresponding region is less dominant compared to that in the left bronchia. This is caused by the smaller angle of deflection of the right bronchia. Regarding the mass flow distribution at steady inspiration the geometry leads to an unbalanced distribution, i.e., the volume flux in the right lung lobe is larger than in the left lobe.

Figure 10 shows the velocity magnitude and velocity profiles at selected positions for steady expiration. The flow is strongly characterized by the inlet velocity from the sub-branches. The velocity profiles in the bronchia possess an M-like shape resulting from the merging fluid jets of the corresponding sub-branches. Due to this effect, the flow cannot develop a parabolic velocity profile but rather possesses a two-peak velocity distribution in the radial direction. This velocity profile represents the inflow condition for the next junction during expiration. The flow

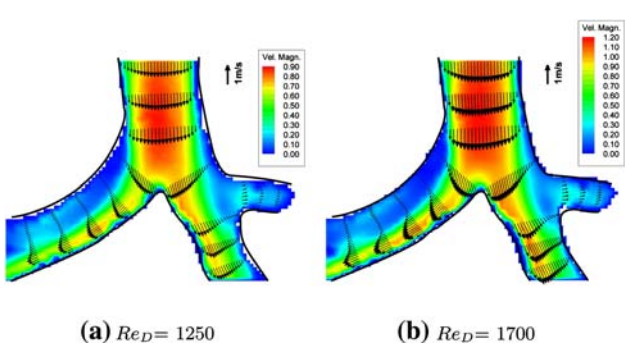

Fig. 8 Velocity profiles at different positions for steady inspiration flow with Re_D = 1,250 and Re_D = 1,700. Contour levels show the vector magnitude

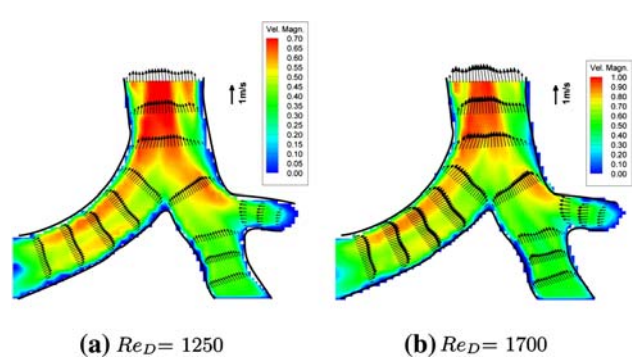

Fig. 10 Velocity profiles at different positions for steady expiration at Re_D = 1,250 and Re_D = 1,700. Contours show the velocity magnitude

following the inner curves possesses higher peak values of the velocity magnitude such that a skewed M-form of the velocity profiles develops. Figure 10 also indicates two small regions in the trachea where the fluid cannot follow the extremely strongly curved wall. Here, the fluid is displaced towards the centerline of the trachea where the peak velocity values occur.

Note, that a quantitative comparison with numerical and for experimental results from the literature is hardly possible due to the varying in- and outflow conditions as well as differing geometries. Especially, variable cross sections, sharp edges and non-matching curvature, are expected to have a strong influence on the flow field in the bifurcation zone. As such, only a very rough comparison of the data can be given.

The existence of regions of reduced velocity with two embedded counter-rotating vortices along the inner curve of the bronchia is also reported by Ramuzat and Riethmuller (2002) for an experimental study of pipe bifurcation flow at Re_D = 1,000 and similar velocity profiles as those in Fig. 8 are found by van Ertbruggen et al. (2005), Yang et al. (2006), and Zhang and Kleinstreuer (2002) for Reynolds numbers ranging from Re_D = 500 to 2,000 also evidencing the existence of a high-speed region close to the lower wall of the bifurcation. The present results and the velocity profiles found in the aforementioned literature confirm a reduced but no reversed mass transport in the region of the two counter-rotating vortices.

Furthermore, the numerical studies by Comer et al. (2001b), and van Ertbruggen et al. (2005) evidence the existence of two counter-rotating vortices by examining the secondary flow field perpendicular to the mean flow direction. This secondary flow pattern corresponds well to the structures found in the present study. Note, that the radial position of the vortex cores within the bronchia does strongly depend on the Reynolds number, the curvature and the sharpness of the bifurcation. Therefore, a quantitative comparison should not be discussed.

3.2 Unsteady flow analysis

3.2.1 Oscillating flow

The measurement at steady flow conditions helps to gain a global understanding of the flow field in the lung. For this reason, many experimental and numerical studies have been performed only for steady flow conditions. However, the results shown in the following demonstrate that it is necessary to account for the unsteady behavior of the flow field during oscillating respiratory ventilation since there is a strong impact of the temporal rate of change of the velocity on the development of the flow field in the bifurcation. Therefore, measurements of oscillating flow have been conducted for a set of parameter combinations of Reynolds number Re_D and Womersley number α where the Reynolds number is based on the maximum bulk velocity at inspiration. This data is summarized in Table 2.

To thoroughly investigate the temporal development of the flow field within the bifurcation region, the velocity field has been visualized in detail. Furthermore, the temporal vorticity distribution within the bifurcation region has been analyzed during inspiration and expiration by visualizing the shear layer between the vortical flow structures in the bifurcation and the remaining high-speed jet. This technique to detect those flow patterns will be explained at length in Sect. 3.2.2.

Figure 11 illustrates the temporal evolution of the out-of-plane vorticity distribution in the central plane in the region of the first bifurcation for Re_D = 1,050 and α = 3.27. The vorticity component is defined as $\omega_y = \frac{\partial u}{\partial z} - \frac{\partial w}{\partial x}$, where u is the horizontal and w the vertical velocity component and x and z are the corresponding Cartesian coordinates in the measurement plane. Narrow bands of increased vorticity identify the extension of the vortices in the left and right bronchia.

During inspiration the Reynolds number increases continuously until it reaches its peak value at approximately 25% of the complete breathing cycle. When the Reynolds number exceeds a critical level, the vortical flow structures described in Sect. 3.1.1 occur in the bronchia. Details of this critical Reynolds number and Womersley number dependence issue and the growth of the vortical structures in the left bronchia, i.e., the aforementioned counter-rotating vortices, will be discussed in Sect. 3.2.2. While this region of vortices in the left bronchia is fed by near-wall fluid from the trachea, the center fluid from the trachea flows straight through the bifurcation and is split at its inner radius (bifurcatio tracheae) following the lower bronchial contour in small streaks of high-speed fluid. The results show depending on the phase in the flow cycle the vortical

Table 2 Investigated parameter combinations of Reynolds number Re_D and Womersley number α

Reynolds no. Re_D (–)	Womersley no. α (–)	Frequency F (cycles/min)	Volumetric flow V (cm^3)
1,050	3.27	10.9	282.6
1,400	3.27	11.0	376.8
2,100	3.27	10.85	565.0
1,050	4.70	22.1	136.3
1,400	4.70	22.3	181.8
2,100	4.70	22.9	272.6
1,050	5.77	34.5	90.6
1,400	5.77	33.2	120.8
2,100	5.77	33.5	181.2

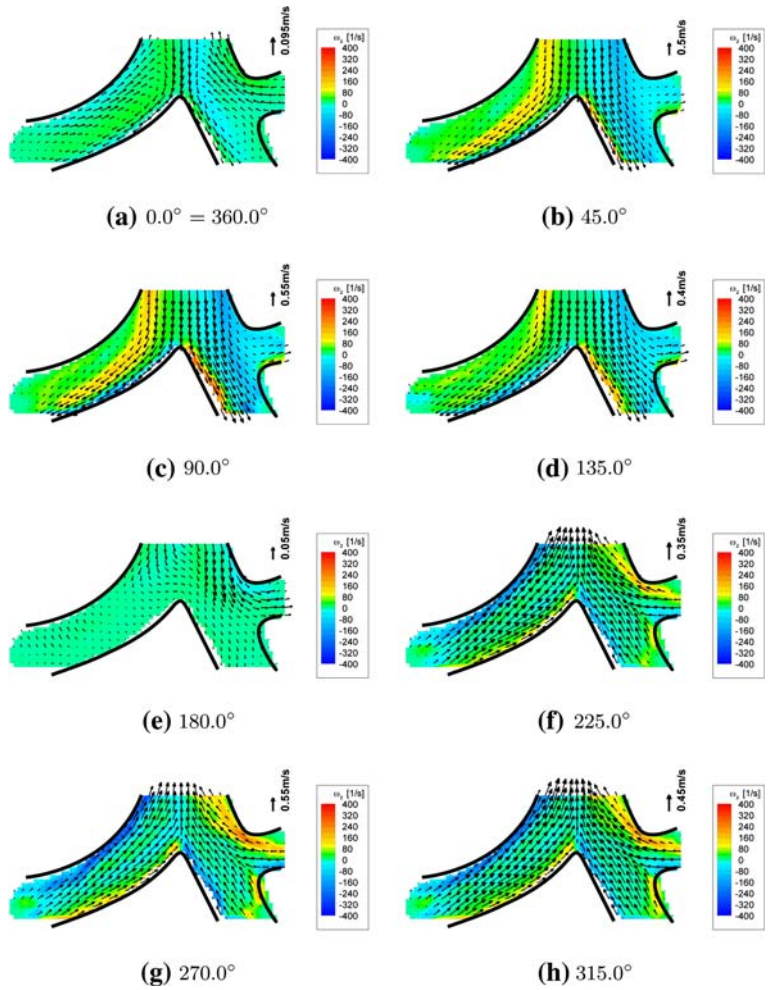

Fig. 11 Temporal evolution of vorticity at different phase angles of the volumetric flow rate. Dorsal view: vector plot of the local velocities. Only every second vector is displayed. Contours represent local vorticity. Inspiration: 11-11, expiration: 11-11, almost no flow: 11, 11

structures along the upper bifurcation wall to change strongly in shape and size at low Reynolds numbers, hence, during their growing phase. Nevertheless, it can be stated that for Reynolds numbers over approximately Re_D = 1,000 the counter-rotating vortices show almost the same extension for all investigated cases.

At the lower end of the two counter-rotating vortices, i.e., nearly three bronchia diameters downstream of the bifurcation, a strong vortical structure can be identified that increases in size and strength when inspiration comes to its end. Before expiration starts, this vortex is pushed outwards by the fluid coming from the daughter branches. During this stage, there is still fluid penetrating into the bronchia close to the lower curvature of the bifurcation, i.e., in the domain in which the high-speed fluid was positioned during inspiration. At the same time, in the region, in which the counter-rotating vortices existed, fluid is already transported to the trachea. It begins to roll up from the lower end of the bronchia generating a strong shear layer between the already reversed flow near the outer bifurcation wall and the remaining inflow of the former high-speed zone. Finally, the latter region is completely suppressed and expiration sets in. In the right bronchia, a dead-water region extends even over the next generation branch. Strong vortical structures also can be identified during the reversal of the flow direction. The complete process is shown in Fig. 12 illustrating in detail four subsequent stages when flow reversal sets in.

During expiration the flow field in the bifurcation and the trachea is strongly influenced by the upstream flow conditions. In Fig. 11g, i.e., at maximum expiration, a centered region of high vorticity is evidenced in the left bronchia. This shear layer results from merging jets of two corresponding sub-branches. Unlike in inspiration, no separation zones can be observed. Only downstream of the trachea a moderate dead water forms on the outer walls. Due to an additional mass flow coming from the upper bronchial branch in the right lobe and due to a more pronounced curvature on the wall the secondary structures on the right side of the trachea are stronger than those on the left side. This also is evidenced in Fig. 10a, b.

When expiration comes to its end, inspiration does not set in uniformly within the bifurcation region. While fluid still flows from the left branch to the trachea, thereby

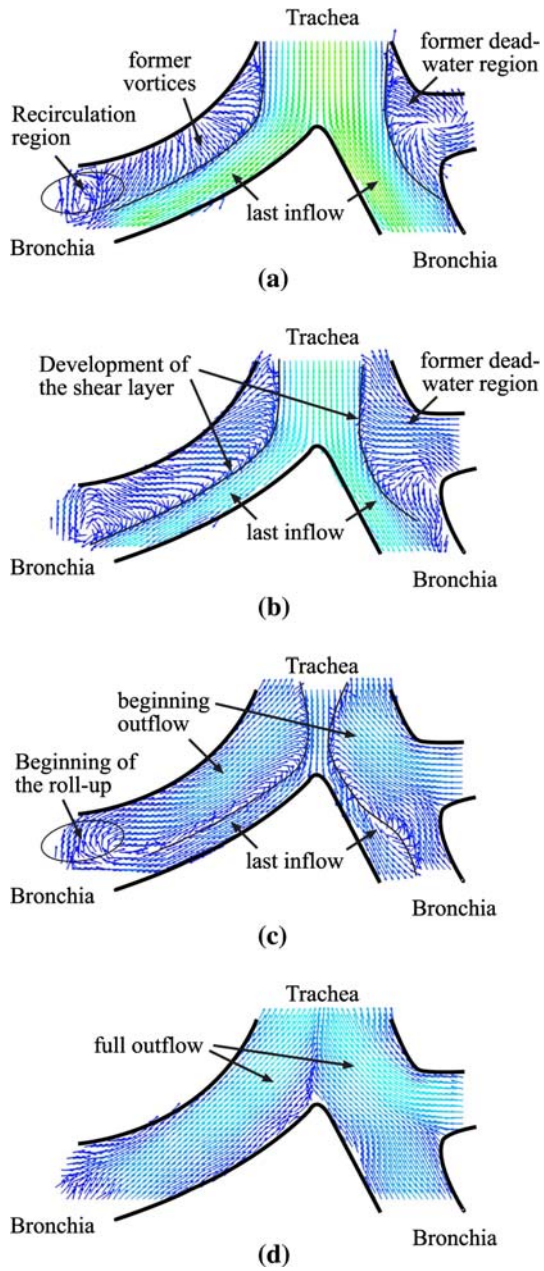

Fig. 12 Characteristic flow structures in the center plane of the first bifurcation at the end of inspiration for four subsequent times. Vectors possess a uniform length, vector colors show the velocity magnitude

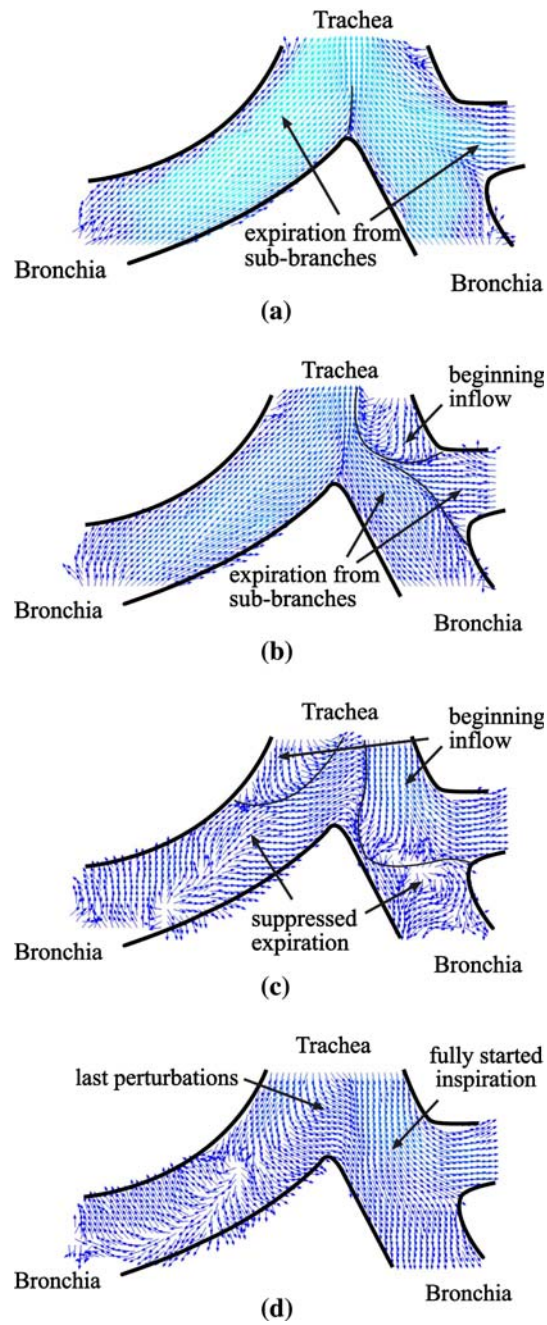

Fig. 13 Characteristic flow structures in the center plane of the first bifurcation at the end of expiration for four subsequent times. Vectors possess a uniform length, vector *colors* show the velocity magnitude

blocking the left part of the trachea, a primary mass flow enters the right bronchia from the trachea. The fluid within the left bronchia begins to stagnate and portions of it are entrained into the right lobe by the fluid entering the lung. At continuing inspiration, the mass flow entering the right lobe increases and, when half the diameter of the trachea is exceeded, fluid also enters the left bronchia in a small region close to the lower curvature of the bifurcation. Finally, the last stagnating fluid from expiration is pushed backwards into the subsequent branches and inspiration starts in the left lobe. The process is shown in Fig. 13 illustrating in detail four subsequent stages when the flow reverses.

3.2.2 Womersley and Reynolds dependence of the vortical flow structures

To investigate the dependence of the secondary flow characteristics in the first bifurcation on the Reynolds and Womersley number, the temporal development of the

vortices has been studied by analyzing the vorticity distribution and by visually determining the flow structures. Several complete flow cycles have been recorded at a frequency of 8 Hz. For an enhanced study of the temporal development of the flow structures, it is useful to sort the recorded data by means of the phase angle within the flow cycle. This reassembling of the data is possible since the flow structures appear periodically during the inspiration cycles. Note, that the sorting of the data is not necessary to evaluate the vorticity distribution. However, the visual identification of the flow field characteristics is simplified by generating such a pseudo temporal resolution. Before actually discussing the results, the post-processing of the data will be described shortly.

Since the recording of the data at oscillating flow was not triggered with the flow cycle, it is necessary to first determine the phase angle of the recorded data within a respiratory cycle. The volumetric flow rate was estimated by the velocity distribution in the trachea. This data was approximated by a sinusoidal curve. From the fitted sinusoidal distribution, the position and as such the phase angle of the recorded data can be determined. Figure 14a exemplarily shows the recorded distribution with the fitted sinusoidal curve and the sorted data (Fig. 14b). Note, that the experimental setup allowed to determine the velocity distribution just in one single plane in the trachea which is why the distribution does not represent a direct measure for the phase angle of the flow cycle. Furthermore, it is evident from Fig. 14a, b that for higher Reynolds numbers the graph of the measured velocity distribution deviates from a sinusoidal curve. The reason for this discrepancy is the deviation of the real velocity profile from a perfect axisymmetric velocity distribution in this area of the bifurcation. The illustrated flow cycle in Fig. 14b is already rescaled with the Reynolds number $Re_{D,\max}$ based on the maximum bulk velocity during inspiration. The distribution starts at inspiration represented by positive values of the Reynolds number. For clarity reasons, i.e., to clearly separate inspiration from expiration, negative values of the Reynolds number are used for the expiration phase.

The investigation of the flow structure was based on the local vorticity distribution that allows to precisely determine the vortical flow structure extension in the bronchia. The location of the maximum value of the vorticity is detected and the average position within the evaluation region of this maximum in relation to the local vertical extension in the bronchia D_V/D_B is determined (Fig. 15). Figure 16 illustrates a representative evolution of this function during a complete flow cycle. Note, that the value shown in Fig. 16 represents the relative one-dimensional extension of the vortical structures averaged over the entire evaluation region in the left bronchia illustrated in Fig. 15.

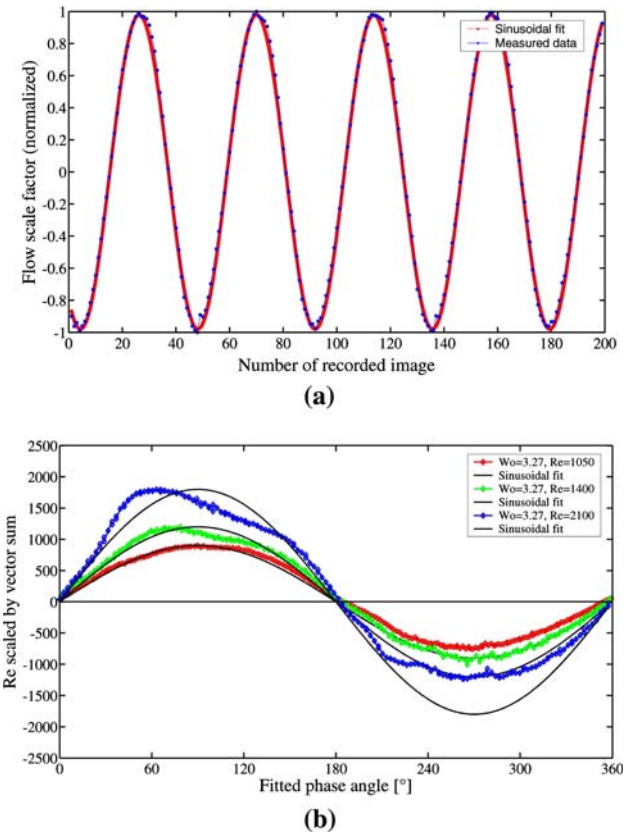

Fig. 14 **a** Recorded time steps during one measurement with the fitted sinusoidal curve. **b** Resorted data rescaled with the maximum Reynolds number $Re_{D,\max}$ during inspiration

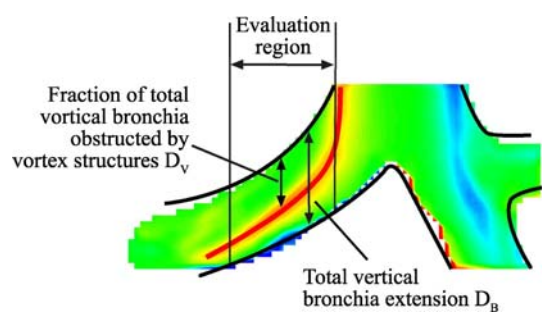

Fig. 15 Schematic of the evaluation of the relative volume of the vortical region. Contours depict the vorticity

In other words, it can be considered a one-dimensional estimate of a volumetric distribution.

We turn now to the discussion of the time dependence, i.e., the Womersley number, on the vorticity distribution decomposed according to Fig. 15 by first elucidating the general temporal evolution of the flow structures within the left bronchia during the inspiration cycle. Since there is a strongly perturbed flow field in the bronchia at the beginning of inspiration, which has been discussed in Sect. 3.2.1, the algorithm finds values of maximum

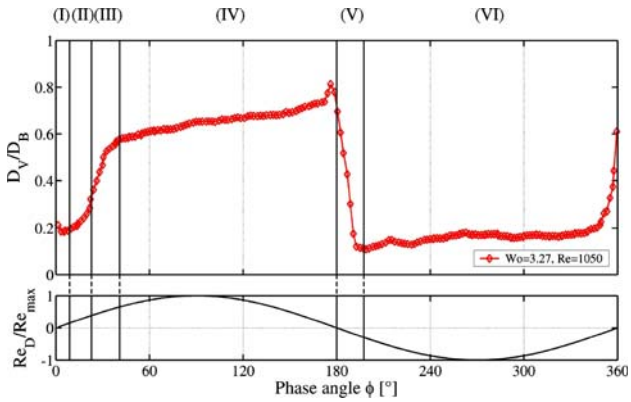

Fig. 16 Temporal evolution of the relative volume of the vortical region at α = 3.27 and Re = 1,050

Table 3 Critical Reynolds number $Re_{D,\ crit}$ for different combinations of Reynolds number Re_D and Womersley number α

Re_D (–)	α (–)	$Re_{D,\ crit}$ (–)	$Re_{D,\ crit}/Re_{D,\ max}$ (–)
1,050	3.27	330	0.32
1,400	3.27	280	0.40
2,100	3.27	370	0.57
1,050	4.70	420	0.20
1,400	4.70	440	0.31
2,100	4.70	470	0.39
1,050	5.77	600	0.18
1,400	5.77	540	0.22
2,100	5.77	480	0.23

vorticity at rather arbitrary positions in the bronchia resulting in a peak of the function in region I in Fig. 16. After this initial phase of the inspiration period, these perturbations disappear and the function reaches a minimum of 0.2 in region II. Then, the increase of the counter-rotating vortical flow structures being independent of the transitional disturbances is initialized. During this stage, fluid is transported in the bronchia quite homogeneously. When the Reynolds number reaches a critical level, the vortical region grows in diameter and extends along the outer radius of the bifurcation into the first bronchia (region III, Fig. 16). This critical Reynolds number $Re_{D,\ crit}$ depends on the Womersley number and the flow rate. The critical Reynolds number is derived from the temporal

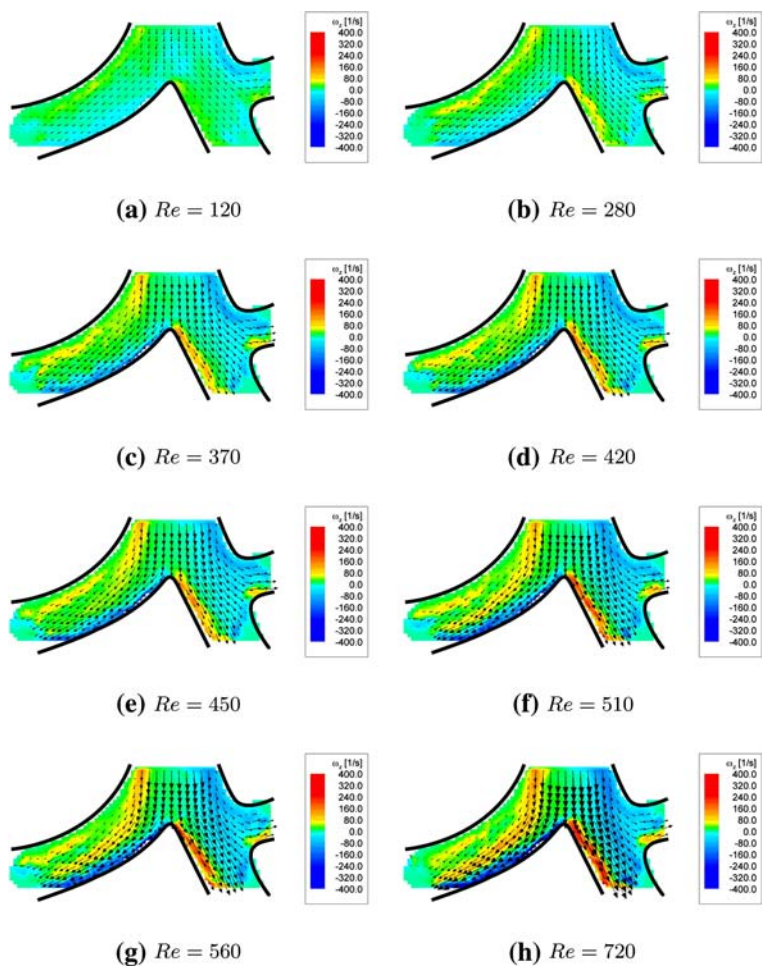

Fig. 17 Vorticity distribution illustrating the temporal evolution of the flow structure during inspiration for α = 3.27 and Re = 1,050. Vectors illustrate the velocity distribution

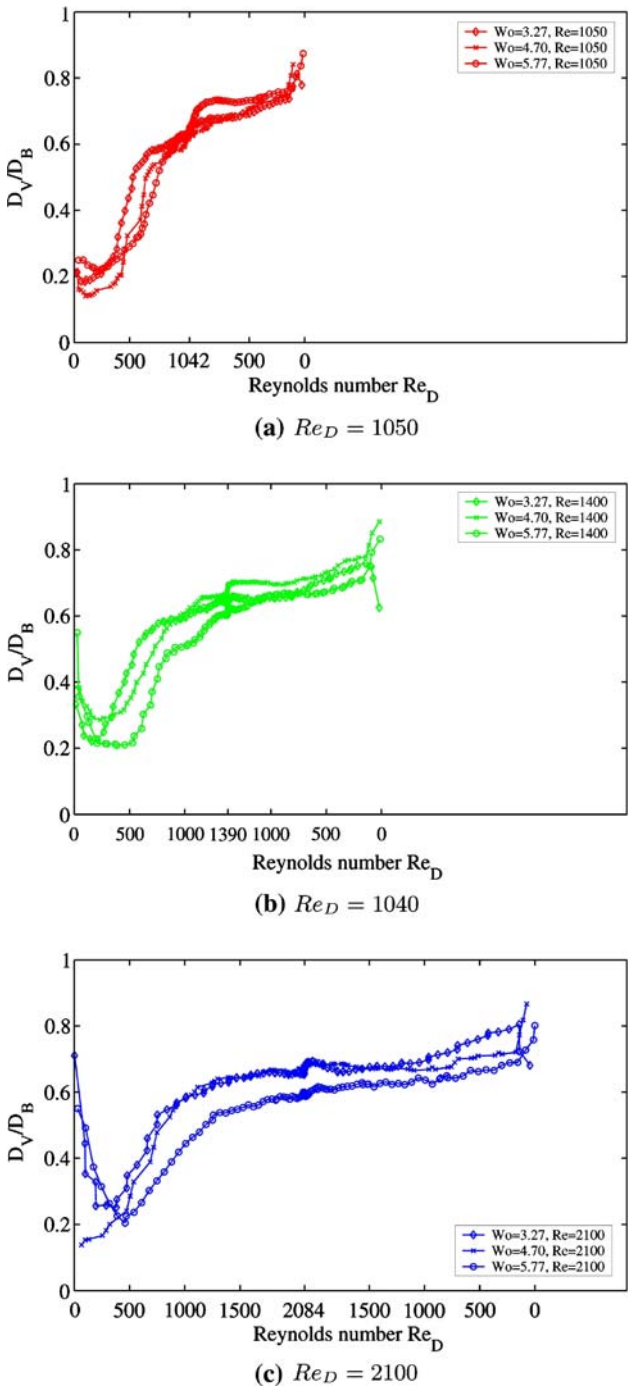

Fig. 18 Relative extension of the vortical region D_V/D_B in the left bronchia as a function of Reynolds and Womersley number

evolution of the position of maximum vorticity. It is defined as the point where the pronounced growth in region III in Fig. 16 sets in. To be more precise, it is the point of intersection of the tangents to the distribution in region II and region III in Fig. 16. Table 3 gives an overview of the values of the Reynolds number at which a strong growth of the structure can be observed.

The spatial structure increases very fast as can be seen in Fig. 16 and reaches almost its final extension after approximately 25% of the total inspiration time. The structure slightly increases in size and the function value rises slowly from 0.6 to 0.7 (region IV in Fig. 16) before it reaches its maximum value $Re_D(t)/Re_{D,\max}$. At the end of inspiration the roll-up process, that has been described in Sect. 3.2.1, washes off these structures (region V in Fig. 16).

Figure 17 exemplarily evidences via the vorticity distribution the growth of these structures in the initial inspiration phase. During expiration there exists no such pronounced vortical region within the left bronchia and consequently, the algorithm finds the vorticity maximum of the shear layer near the boundaries. Hence, during expiration, the value of the vortical extension D_V/D_B remains constantly at a low level of 0.2 (region VI in Fig. 16).

A comparison of the flow structure development during inspiration for different combinations of Reynolds and Womersley numbers evidences a strong impact of the Womersley number on the temporal development of the secondary flow vortices. It is evidenced from Table 3 and Fig. 18 that the critical Reynolds number $Re_{D,\,\mathrm{crit}}$ increases at higher Womersley number for a constant maximum Reynolds number $Re_{D,\max}$ during inspiration. That is, the development of the vortical flow structure is delayed, whereas the maximum extent is hardly affected by changing the flow parameters since the range of the relative extension $0.6 \leq D_V/D_B \leq 0.7$ is rather small. From the evolution of the vortical region as a function of the dimensionless Reynolds number $Re_D(t)/Re_{D,\max}$ in Fig. 19, it can further be conjectured that at constant Womersley number higher maximum Reynolds numbers $Re_{D,\max}$ lower the critical Reynolds number at constant Womersley number.

These results clearly demonstrate that not only the Reynolds number defines the characteristics of the flow field in the first bifurcation. It is rather evident that the unsteady character of the flow field plays a likewise significant role on the development of the flow in the first bifurcation region.

4 Conclusion and outlook

Velocity measurements of steady inspiration and expiration at two Reynolds numbers of Re_D = 1,250 and Re_D = 1,700 were presented. The results evidenced the Reynolds number of the flow to play a minor role on the extension of the flow phenomena. For both Reynolds numbers, very similar flow structures could be observed at steady inspiration. To be more precise, especially the size of the counter-rotating vortical structures did not depend on the Reynolds number

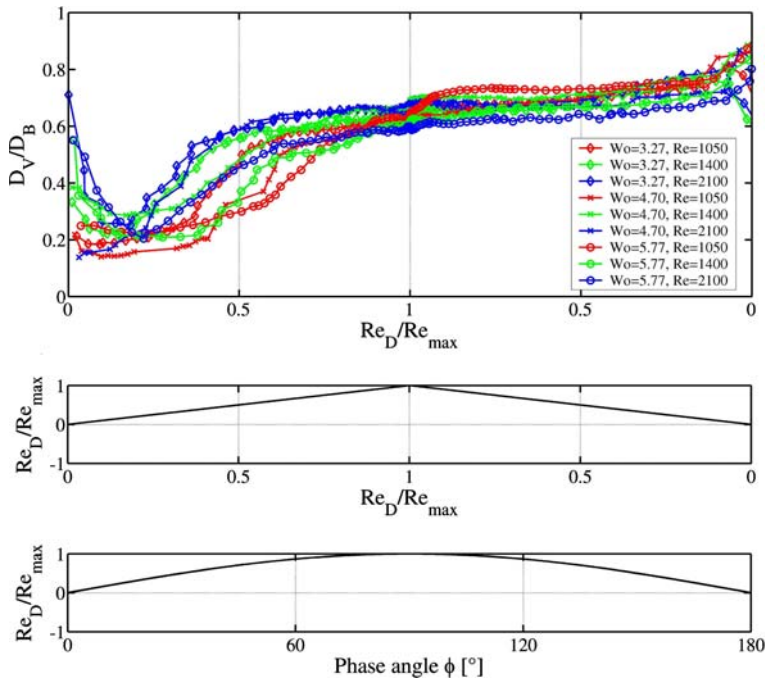

Fig. 19 Relative extension of the vortical region D_V/D_B in the left bronchia as a function of Reynolds and Womersley number

as long as this Reynolds number was above a critical level of roughly Re_D = 800–1,200.

The measurements at unsteady flow corroborate the flow characteristics to be completely different from the steady flow field. In other words, as expected, the Womersley number of the flow plays a major role on the development of the flow structures in the bifurcation.

The oscillating flow studies show the size of the evolving secondary flow structures to rather strongly depend on the instantaneous Reynolds number and the Womersley number. A highly intricate flow structure consisting of a spiral-like trajectory was found in a region along the upper wall of the left branch of the first bifurcation. The results from the oscillating flow experiments demonstrate the importance of the unsteady character of the flow field. The investigations indicated the vortical flow regions at inspiration to strongly change in shape and size due to the local acceleration of the flow at low Reynolds numbers, or in other words, due to the time-dependence of the velocity. In brief, at higher Womersley number, the critical Reynolds number is increased and at higher Reynolds number the critical Reynolds number, which describes the onset of strong vortical structures in the first bifurcation, is decreased.

At expiration the unsteady and steady flow solutions are more similar than at inspiration since hardly any major secondary flow structures are observed. Consequently, this study shows that it is necessary to investigate the evolution of a realistic bronchial flow in experiments with oscillating flow, since steady experiments do not allow to simulate the temporal development of the flow which, however, determines the overall flow structure.

Despite the three-dimensional character of the flow field within the bifurcation it has been shown that the large-scale geometry of the secondary flow structures can be approximately derived from a single measurement plane located at the center plane of the bifurcation. Nonetheless, a quantitative evaluation of volumetric flow rates will require a time-resolved three-dimensional measurement of the flow field.

Furthermore, from the presented results it can be clearly concluded that the characteristic length of the bronchial generations is too short to achieve fully developed flow profiles before entering the next generation of bronchia. Therefore, special care has to be taken when flow rate distributions in this highly complex geometry are to be determined.

In the future, further measurements in subsequent generations of the lung geometry will be used to analyze to what extent the upstream flow conditions have an impact on the flow field in corresponding sub-branches as a function of the local Reynolds number. Additionally, a more realistic inflow should be examined by incorporating the laryngeal region of the upper human airways in the model such that the flow entering the lung will have experienced likewise upstream conditions as the real human lung flow. Furthermore, it has to be investigated whether a defined pressure distribution at the end of the 6th generations' branches and controlled flow volumes for each of these branches possess an influence on the flow field of the upper airways.

Finally, the flow field during high-frequency oscillatory ventilation (HFV) with ventilation frequencies between 5

and 15 Hz will be investigated, since this technique has reached increasing clinical applications and the already-conducted oscillating flow measurements at high Womersley number showed a strongly retarded evolution of secondary flow structures in the bifurcation. The global effect of this behavior still needs to be investigated.

References

Ball CG, Uddin M, Pollard A (2006) Lattice Bolzmann simulation of flow in the human upper airway. In: Proceedings of the 5th conference on turbulence, heat and mass transfer, pp 305–308

Caro CG, Schroter RC, Watkins N, Sherwin SJ, Sauret V (2002) Steady inspiratory flow in planar and non-planar models of human bronchial airways. R Soc Lond Proc Series A 458:791–809

Comer JK, Kleinstreuer C, Hyun S, Kim CS (2000) Aerosol transport and deposition in sequentially bifurcating airways. Trans ASME J Biomech Eng 122(2):152–158

Comer JK, Kleinstreuer C, Kim CS (2001a) Flow structures and particle deposition patterns in double-bifurcation airway models. Part 2. Aerosol transport and deposition. J Fluid Mech 435:55–80

Comer JK, Kleinstreuer C, Zhang Z (2001b) Flow structures and particle deposition patterns in double-bifurcation airway models. Part 1. Air flow fields. J Fluid Mech 435:25–54

van Ertbruggen C, Hirsch C, Paiva M (2005) Anatomically based three-dimensional model of airways to simulate flow and particle transport using computational fluid dynamics. J Appl Physiol 98:970–980

Große S, Schröder W, Klaas M (2007) Time-resolved PIV measurements of vortical structures in the upper human airways. Accepted for publication in Topics Applied Physics

Grotberg JB (2001) Respiratory fluid mechanics and transport processes. Annu Rev Biomed Eng 3:421–457

Leong FY, Smith KA, Wang CH (2005) Transport of sub-micron aerosols in bifurcations. In: Proceedings of molecular engineering of biological and chemical systems (MEBCS)

Liu Y, So RMC, Zhang CH (2003) Modeling the bifurcating flow in an asymmetric human lung airway. J Biomech 36:951–959

Martonen T (2001) Commentary 'Effects of asymmetric branch flow rates on aerosol deposition in bifurcating airways', by Zhang Z, Kleinstreuer C and Kim CS. J Med Eng Technol 25(3):124–126

Martonen TB, Guan X, Schreck RM (2001) Fluid dynamics in airway bifurcations: II. Secondary currents. Inhal Toxicol 13:281–289

Mochzuki S (2003) Convective mass transport during ventilation in a model of branched airways of human lungs. In: Proceedings of the 4th Pacific symposium on flow visualization and image processing (PSFVIP4), Chamonix, France, 3–5 June 2003

Ramuzat A, Riethmuller ML (2002) PIV investigation of oscillating flows within a 3D lung multiple bifurcations model. In: Proceedings of the 11th international symposium on applications of laser techniques to fluid mechanics, Lisbon, Portugal, 8–11 July 2002, pp 19.1.1.–19.1.10

Robinson RJ, Oldham MJ, Clinkenbeard RE, Rai P (2006) Experimental and numerical smoke carcinogen deposition in a multi-generation human replica tracheobronchial model. Ann Biomed Eng 34(3):373–383

Schroter RC, Sudlow MF (1969) Flow patterns in models of the human bronchial airways. Respir Physiol 7:341–355

Weibel ER (1963) Morphometry of the human lung. Springer, Berlin

Yang XL, Liu Y, So RMC, Yang JM (2006) The effect of inlet velocity profile on the bifurcation COPD airway flow. Comput Biol Med 36:181–194

Zhang Z, Kleinstreuer C (2002) Transient airflow structures and particle transport in a sequentially branching lung airway model. Phys Fluids 14(2):862–880